

## Genitourinary Imaging

Juergen Scheidler, MD  
Hedvig Hricak, MD, PhD  
Daniel B. Vigneron, PhD  
Kyle K. Yu, MD  
Dahlia L. Sokolov, BS  
L. Royal Huang, BS  
Charles J. Zaloudek, MD  
Sarah J. Nelson, PhD  
Peter R. Carroll, MD  
John Kurhanewicz, PhD

### Index terms:

Magnetic resonance (MR),  
spectroscopy, 844.12145  
Magnetic resonance (MR), three-  
dimensional, 844.12149  
Prostate, hyperplasia, 844.316  
Prostate, MR, 844.12141, 844.12145  
Prostate, neoplasms, 844.32

**Radiology** 1999; 213:473-480

### Abbreviations:

$A_z$  = area under the receiver  
operating characteristic curve  
ROC = receiver operating  
characteristic  
3D = three-dimensional

<sup>1</sup> From the Departments of Radiology (J.S., H.H., D.B.V., K.K.Y., D.L.S., L.R.H., S.J.N., J.K.), Pathology (C.J.Z.), and Urology (P.R.C.), University of California at San Francisco, 505 Parnassus Ave, San Francisco, CA 94143-0628. From the 1997 RSNA scientific assembly. Received April 23, 1998; revision requested July 2; final revision received February 24, 1999; accepted June 8. J.S. supported by the Deutsche Forschungsgemeinschaft. J.K. supported by grants RO1-59897 and R29-64667 from the National Institutes of Health. K.K.Y. supported by a GE-AUR Radiology Research Academic Fellowship. **Address reprint requests to J.K.** (e-mail: [johnk@mrsc.ucsf.edu](mailto:johnk@mrsc.ucsf.edu)).

© RSNA, 1999

See also the article by Yu et al (pp 481-488) in this issue.

### Author contributions:

Guarantor of integrity of entire study, H.H.; study concepts and design, H.H., J.S., J.K.; definition of intellectual content, H.H., J.K.; literature research, J.S.; clinical studies, J.S., P.R.C.; data acquisition, J.S., H.H., D.B.V., D.L.S., L.R.H., C.J.Z., S.J.N., J.K.; data analysis, J.S., K.K.Y.; statistical analysis, J.S., K.K.Y.; manuscript preparation, J.S., K.K.Y., H.H.; manuscript editing, K.K.Y., H.H.; manuscript review, D.B.V., P.R.C., J.K., S.J.N.

# Prostate Cancer: Localization with Three-dimensional Proton MR Spectroscopic Imaging—Clinicopathologic Study<sup>1</sup>

**PURPOSE:** To assess the efficacy of combined magnetic resonance (MR) imaging and three-dimensional (3D) proton MR spectroscopic imaging in the detection and localization of prostate cancer.

**MATERIALS AND METHODS:** MR imaging and 3D MR spectroscopic imaging examinations were performed in 53 patients with biopsy-proved prostate cancer and subsequent radical prostatectomy with step-section histopathologic examination. The prostate was divided into sextants. At MR imaging, the presence or absence of cancer in the peripheral zone of each sextant was assessed independently by two readers (readers 1 and 2) unaware of the findings at 3D MR spectroscopic imaging and histopathologic examination. At 3D MR spectroscopic imaging, cancer was diagnosed as possible if the ratio of choline plus creatine to citrate exceeded 2 SD above population norms or as definite if that ratio exceeded 3 SDs above the norm.

**RESULTS:** On the basis of sextants, sensitivity and specificity, respectively, for MR imaging were 77% and 61% (reader 1) and 81% and 46% (reader 2) with moderate interreader agreement ( $\kappa = 0.43$ ). The 3D MR spectroscopic imaging diagnosis of definite cancer had significantly higher specificity (75%,  $P < .05$ ) but lower sensitivity (63%,  $P < .05$ ). Receiver operating characteristic analysis showed significantly ( $P < .001$ ) improved tumor localization for both readers when 3D MR spectroscopic imaging was added to MR imaging. High specificity (up to 91%) was obtained when combined MR imaging and 3D MR spectroscopic imaging indicated cancer, whereas high sensitivity (up to 95%) was obtained when either test alone indicated a positive result.

**CONCLUSION:** The addition of 3D MR spectroscopic imaging to MR imaging provides better detection and localization of prostate cancer in a sextant of the prostate than does use of MR imaging alone.

The rising incidence of prostate cancer (estimated incidence in 1985, 86,000 new cases; 1997, 209,900 new cases) (1,2) and the aging population have made prostate cancer an important medical and socioeconomic problem. The increase in prostate cancer incidence is likely related to an increase in screening with digital rectal examination, measurement of prostate-specific antigen, and use of transrectal ultrasonography (US) and biopsy (3). Between 1990 and 1997, however, the mortality from prostate cancer also increased (estimated increase, 39%) (4), which suggests a true increase in clinically important disease.

Surgery and radiation therapy represent the mainstays of prostate cancer treatment. The emerging concept of patient-specific localized tumor therapy aims to improve patient outcome by maintaining treatment efficacy while reducing treatment-associated morbidity. In this context, the accurate localization of prostate cancer within the prostate gland is becoming increasingly important, as it can affect surgical and radiation treatment planning and can guide the extent of cryosurgery. Furthermore, the choice of a watchful waiting strategy can be assisted with knowledge of tumor size and growth. The development of patient-specific therapy is limited by the inability of current diagnostic techniques to differentiate aggressive from indolent cancer and to accurately localize and stage this disease.

Transrectal US is widely used for guidance of prostate gland biopsy, but sensitivity and specificity are low in the localization of prostate cancer. Magnetic resonance (MR) imaging has a significantly higher sensitivity for tumor detection than does transrectal US but, like transrectal US, has low specificity (5–10). The addition of metabolic information from three-dimensional (3D) MR spectroscopic imaging to morphologic data from MR imaging may allow more specific diagnosis and localization of prostate cancer. MR spectroscopy has been used to obtain metabolic data from tumors in situ (11,12). Recent technical developments have allowed the application of localized three-dimensional proton 3D MR spectroscopic imaging to the in vivo evaluation of the human prostate (13). With use of 3D MR spectroscopic imaging, significantly higher choline levels and significantly lower citrate levels were observed in regions of cancer compared with areas of benign prostatic hypertrophy and normal prostatic tissue. The ratio of these metabolites (choline to citrate) in regions of cancer appears not to overlap with ratios in the normal peripheral zone, which suggests that 3D MR spectroscopic imaging combined with MR imaging may improve tumor detection and localization compared to those with MR imaging alone (13). Feasibility and technical development of prostatic 3D MR spectroscopic imaging have been reported (13), but the efficacy of 3D MR spectroscopic imaging in prostate cancer detection or combined results with MR imaging and 3D MR spectroscopic imaging data in the detection or localization of prostate cancer have not been described, to our knowledge.

The purpose of this study was to assess the effectiveness of combined 3D MR spectroscopic imaging and MR imaging for tumor detection and localization with results at step-section histopathologic examination as the standard of reference.

## MATERIALS AND METHODS

### Patients

This was a retrospective cross-sectional study. Between May 1992 and June 1997, 517 consecutive patients with biopsy-proved prostate cancer were referred for combined endorectal and phased-array coil MR imaging and 3D MR spectroscopic imaging. Eighty-nine patients subsequently underwent radical prostatectomy at our institution. Medical records, MR imaging and 3D MR spectroscopic imaging studies, and histopathologic data were reviewed. Thirty-six patients were

excluded because (a) results at step-section histopathologic examination were not available for review ( $n = 2$ ); (b) at step-section histopathologic examination, prostate cancer was not located in the peripheral zone ( $n = 3$ ); (c) MR images or 3D MR spectroscopic imaging data could not be retrieved or photographed ( $n = 11$ ); (d) 3D MR spectroscopic imaging signal-to-noise ratio was nondiagnostic ( $n = 5$ ); or (e) radical prostatectomy was performed more than 3 months after MR imaging and 3D MR spectroscopic imaging studies ( $n = 6$ ). Nine patients had undergone androgen-deprivation therapy (a potentially confounding factor) before the combined MR imaging and 3D MR spectroscopic imaging examination (14), and they were also excluded from further analysis. The remaining 53 patients formed the study population.

Mean patient age was  $60.2 \text{ years} \pm 7.1$  (SD). Mean preoperative prostate-specific antigen was  $8.2 \text{ ng/mL} \pm 5.0$ . The mean interval between the MR examination and radical retropubic prostatectomy was  $28.4 \text{ days} \pm 23.0$  (range, 1–86 days).

### MR Imaging Technique

MR imaging was performed with a 1.5-T MR imaging system (Signa; GE Medical Systems, Milwaukee, Wis). The endorectal coil (Medrad, Pittsburgh, Pa) was connected to the pelvic phased-array coil, and combined images were obtained. After acquisition of a sagittal T2-weighted fast spin-echo localizer image to check coil position, transverse T2-weighted fast spin-echo images were obtained from below the apex of the prostate to above the seminal vesicles with the following parameters: repetition time msec/echo time msec (effective) of 4,000–5,000/102, 3-mm section thickness, no intersection gap, three signals acquired, 14-cm field of view,  $256 \times 192$  matrix, no phase wrap. Transverse T1-weighted images (500–700/12, 4-mm-thick sections, 1-mm section gap, two signals acquired, 14-cm field of view,  $256 \times 192$  matrix, no phase wrap) were then obtained from below the apex of the prostate to the level of the aortic bifurcation to assess for sites of postbiopsy bleeding and pelvic lymphadenopathy. All images were analytically corrected for the reception profile of the endorectal and pelvic phased-array coils (15). The total examination time, including patient positioning, coil placement, MR imaging, and 3D MR spectroscopic imaging, was typically 50–60 minutes.

### Three-dimensional MR Spectroscopic Imaging Protocol

The 3D MR spectroscopic imaging technique has been previously described in detail (13,16,17). In brief, from the high-spatial-resolution transverse T2-weighted images, a spectroscopic volume was selected with the point-resolved spectroscopic, or PRESS, technique to encompass as much of the prostate as possible, while excluding periprostatic fat. The echo delay of the point-resolved spectroscopic sequence (130 msec) was optimized for the quantitative detection of both citrate and choline. The position of the selected volume and the accuracy of localization were evaluated by means of MR imaging. A 3D MR spectroscopic imaging data set was acquired with a spatial resolution of  $0.24\text{--}0.70 \text{ cm}^3$ . Studies were performed with 1,000/130, a spectral width of 1,250 Hz, 512 points,  $8 \times 8 \times 8$  phase-encoding steps with two signals or  $16 \times 8 \times 8$  with one signal acquired per phase-encoding step, yielding 512 or 1,024 proton MR spectra, respectively, of which between 40 and 332 were from within the prostate, depending on gland size and spatial resolution. Technical improvements during the study resulted in improved cranio-caudal coverage of the peripheral zone of the prostate gland, which was increased from 20%–50% to 70%–100%. For this study, 3D MR spectroscopic imaging provided peripheral zone coverage of less than 25% in one patient, 25.0%–49.9% in 17 patients, 50.0%–74.9% in 23 patients, and 75%–100% in 12 patients.

### MR Image Analysis

All images were interpreted retrospectively by two independent readers (H.H., K.K.Y.) unaware of clinical, 3D MR spectroscopic imaging, and histopathologic findings. Both readers knew that all patients had biopsy-proved prostate cancer. Reader 1 was more experienced than reader 2 and had interpreted at least twice the number of prostatic studies (at least 500 over the preceding 5 years).

To allow for direct comparison between MR imaging and 3D MR spectroscopic imaging, MR image evaluation was performed on only sections covered at 3D MR spectroscopic imaging. The presence of cancer, identified as an area of low signal intensity within the peripheral zone on T2-weighted images, was recorded for each section by each of the two readers independently and entered on a standardized form developed for this study. For each examination, the likelihood of tu-

mor presence was estimated with a 5-point rating scale: 1, normal tissue; 2, probably normal tissue; 3, possible cancer; 4, probable cancer; 5, definite cancer. For calculation of sensitivity and specificity, these results were dichotomized so that cancer was diagnosed for scores 4 and 5 and was not diagnosed for scores 1–3.

### Three-dimensional MR Spectroscopic Imaging Data Processing

All 3D MR spectroscopic imaging data were transferred off-line and processed on an UltraSparc workstation (Sun Microsystems, Mountain View, Calif) with software developed for 3D MR spectroscopic imaging studies. The spectral data sets were apodized with a 2-Hz Lorentzian function and were Fourier transformed in the time domain and three spatial domains. After frequency, phase, and baseline correction (16), the integral areas for the choline, creatine, and citrate resonances were calculated (13,16). In addition to the peak parameters, the quantification algorithm was also used to estimate random noise and, hence, the accuracy of the estimates of peak metabolite areas. To discriminate between cancer and normal prostatic tissue in the peripheral zone, we calculated the peak area ratios of choline plus creatine to citrate and citrate to normal citrate for each voxel (13). These ratios and the signal-to-noise ratios for choline and citrate were reported as the mean plus or minus SD. Possible cancer was defined as voxels with a ratio of choline plus creatine to citrate of greater than 2 SD above normal ( $>0.75$ ) or a twofold decrease in citrate over normal citrate as determined in a previous study (13). Definite cancer was identified when the ratio of choline plus creatine to citrate was greater than 3 SD above normal ( $>0.86$ ). Voxels with a ratio of choline plus creatine to citrate of less than 0.75 were considered normal peripheral zone tissue. To enable receiver-operating-characteristic (ROC) analysis, the same rating scale used for MR imaging was used for 3D MR spectroscopic imaging.

To correlate metabolic data with anatomy and histopathologic findings within the same study, data were displayed by plotting proton spectral arrays on the corresponding transverse T2-weighted images. The 3D MR spectroscopic imaging phase-encoding grid and the outline of the selected volume were superimposed on the T2-weighted images. The use of the same gradients and the same patient position within a study allowed alignment of

MR imaging and 3D MR spectroscopic imaging data.

### Histopathologic Review

After surgical resection, the prostate gland was coated with India ink and fixed in 10% buffered formaldehyde. The gland was transversely sectioned at 3–4-mm intervals in a plane perpendicular to the long axis (base to apex) of the gland. Presence, location, and extent of cancer was determined and entered on standardized histopathologic forms with diagrams that corresponded to the MR imaging data forms.

Mean surgical histopathologic Gleason score was  $5.3 \pm 1.0$  (range, 4–10). Unilateral disease was present in 14 patients, and bilateral multifocal cancer was present in 39 (74%). At histopathologic analysis, 38 of 53 patients (72%) had disease confined to the gland (stage pT2a, five patients; stage pT2b, four patients; stage pT2c, 29 patients). Twelve patients had unilateral extracapsular extension (stage pT3a), one patient had bilateral extracapsular extension (stage pT3b), and two patients had seminal vesicle invasion (stage pT3c).

### Correlation of MR Imaging and 3D MR Spectroscopic Imaging Findings with Histopathologic Findings

One of the authors (J.S.), who was not a reader of either MR imaging or 3D MR spectroscopic imaging data, assembled all of the images for interpretation, maintained the database of histopathologic information, and correlated MR imaging and 3D MR spectroscopic imaging findings with the results at histopathologic examination. The correlation was performed on a section-by-section basis. However, the definition of matching sections was complicated by differences in technique. In particular, the angle at which the histopathologic sections were cut often differed from the angle at which imaging was performed (difference of  $5^\circ$ – $20^\circ$ ). The size and shape of the prostate may also change as a result of tissue shrinkage during fixation. MR and 3D MR spectroscopic images were acquired with 3-mm section thickness without gap, whereas histopathologic slices were 5-mm thick and made every 3–4 mm. To correct for these differences in sectioning technique, a tumor site on MR or 3D MR spectroscopic images was considered to match the histopathologic site if the tumor was present in the peripheral zone of

the same sextant of the prostate (right or left base, right or left middle gland, right or left apex) within a range of one section (craniocaudal distance,  $\pm 3$ – $4$  mm). In addition, the tumor had to be in the same anterior or posterior location. Sections through the bladder neck and proximal prostatic urethra were considered the prostatic base, whereas the prostatic apex was defined on the basis of the doughnut-like appearance of the distal prostatic urethra. The remainder of the prostate was considered the middle gland. Data analysis included evaluation of the ability of MR imaging and 3D MR spectroscopic imaging to localize tumor to a sextant or side of the prostate.

### Statistical Analysis

Descriptive statistics included sensitivity and specificity with their corresponding 95% CIs and positive and negative predictive values for each test. The McNemar test was used to determine whether there were any statistically significant ( $P < .05$ ) differences in diagnostic accuracy between MR imaging and 3D MR spectroscopic imaging for both readers. Complementarity of MR imaging and 3D MR spectroscopic imaging results was assessed by calculating the 95% CIs for the probability that 3D MR spectroscopic imaging can depict or exclude additional tumor sites compared with findings at MR imaging (18). ROC analysis was used to compare the results at MR imaging to those with the combination of MR imaging and 3D MR spectroscopic imaging. Results of MR imaging and 3D MR spectroscopic imaging were combined by adding the MR imaging result (scores 1–5 in the rating scale) to the 3D MR spectroscopic imaging ratings (scores 1, 3, and 5 in the rating scale). The method of Hanley and McNeil was used for the paired testing of significance of difference in area under the ROC curve ( $A_z$ ) (19). Interreader agreement on MR image interpretation was quantified with  $\kappa$  statistics, with  $\kappa$  less than 0.4 considered poor agreement,  $\kappa$  between 0.40 and 0.75 considered good agreement, and  $\kappa$  greater than 0.75 considered excellent agreement.

## RESULTS

### Overall Performance of MR Imaging and 3D MR Spectroscopic Imaging

Two-hundred thirty-four of 318 available sextants were covered at 3D MR spectroscopic imaging, and they formed the database for correlation with step-

**TABLE 1**  
**Comparison of MR Imaging and 3D MR Spectroscopic Imaging for Tumor Detection on a Sextant-by-Sextant Basis (right and left base, middle gland, apex)**

Modality and Finding	Sensitivity (%)	Specificity (%)	Positive Predictive Value (%)	Negative Predictive Value (%)	Accuracy (%)
MR imaging					
Reader 1	77 (120 of 155)	61 (48 of 79)	79 (120 of 151)	58 (48 of 83)	72 (168 of 234)
95% CI	72, 83	55, 67	74, 85	52, 64	66, 78
Reader 2	81 (125 of 155)	46 (36 of 79)	74 (125 of 168)	55 (36 of 66)	69 (161 of 234)
95% CI	76, 86	39, 52	69, 80	48, 61	63, 75
3D MRSI					
Prostate cancer definite	63 (98 of 155)	75 (59 of 79)*	83 (98 of 118)	51 (59 of 116)	67 (157 of 234)
95% CI	57, 69	69, 80	78, 88	44, 57	61, 73
Prostate cancer possible	86 (134 of 155)	49 (39 of 79)	77 (134 of 174)	65 (39 of 60)	74 (173 of 234)
95% CI	82, 91	43, 56	72, 82	59, 71	68, 80

Note.—MRSI = MR spectroscopic imaging. Data in parentheses are the number of prostatic lobes.

\*  $P < .05$  compared with MR imaging.

**TABLE 2**  
**Comparison of MR Imaging and 3D MR Spectroscopic Imaging for Tumor Lateralization (right or left prostatic lobe)**

Modality and Finding	Sensitivity (%)	Specificity (%)	Positive Predictive Value (%)	Negative Predictive Value (%)	Accuracy (%)
MR imaging					
Reader 1	89 (82 of 92)	43 (6 of 14)	91 (82 of 90)	38 (6 of 16)	83 (88 of 106)
95% CI	83, 95	33, 52	86, 97	28, 47	76, 90
Reader 2	88 (81 of 92)	29 (4 of 14)	89 (81 of 91)	27 (4 of 15)	80 (85 of 106)
95% CI	82, 94	20, 37	83, 95	18, 35	73, 88
3D MRSI					
Prostate cancer definite	77 (71 of 92)	64 (9 of 14)*	93 (71 of 76)	30 (9 of 30)	75 (80 of 106)
95% CI	69, 85	55, 73	89, 98	21, 39	67, 84
Prostate cancer possible	96 (88 of 92)	36 (5 of 14)	91 (88 of 97)	56 (5 of 9)	88 (93 of 106)
95% CI	92, 100	27, 45	85, 96	46, 65	81, 94

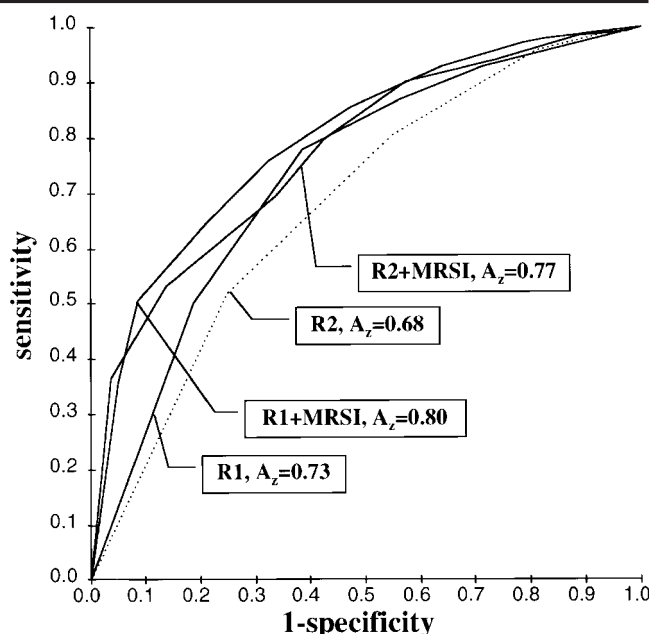
Note.—MRSI = MR spectroscopic imaging. Data in parentheses are the number of prostatic lobes.

\*  $P < .05$  compared with MR imaging.

section histopathologic examination findings. Histopathologic correlation revealed prostate cancer in 155 of 234 sextants.

Tables 1 and 2 summarize the results of MR imaging and 3D MR spectroscopic imaging on a sextant-by-sextant basis (Table 1) and for tumor lateralization (Table 2). Although there were no significant differences in diagnostic accuracy between readers 1 and 2 with MR imaging, ROC analysis revealed significantly ( $P < .01$ ) better performance of reader 1 ( $A_z = 0.73$ ) compared with reader 2 ( $A_z = 0.68$ ) (Fig 1). Interreader agreement for tumor detection was moderate ( $\kappa = 0.43$ ). When the MR imaging results of readers 1 and 2 were compared to their results with 3D MR spectroscopic imaging for definite cancer, there was a trend toward higher sensitivity with MR imaging (both readers) and higher specificity with 3D MR spectroscopic imaging. Figures 2 and 3 show sample MR images with the corre-

**Figure 1.** ROC curves with MR imaging for reader 1 (R1) and reader 2 (R2) and with combined MR imaging and 3D MR spectroscopic imaging for reader 1 (R1 + MRSI) and reader 2 (R2 + MRSI). The  $A_z$  values with combined MR imaging and 3D MR spectroscopic imaging for both readers were significantly ( $P < .001$ ) greater than those with MR imaging alone.



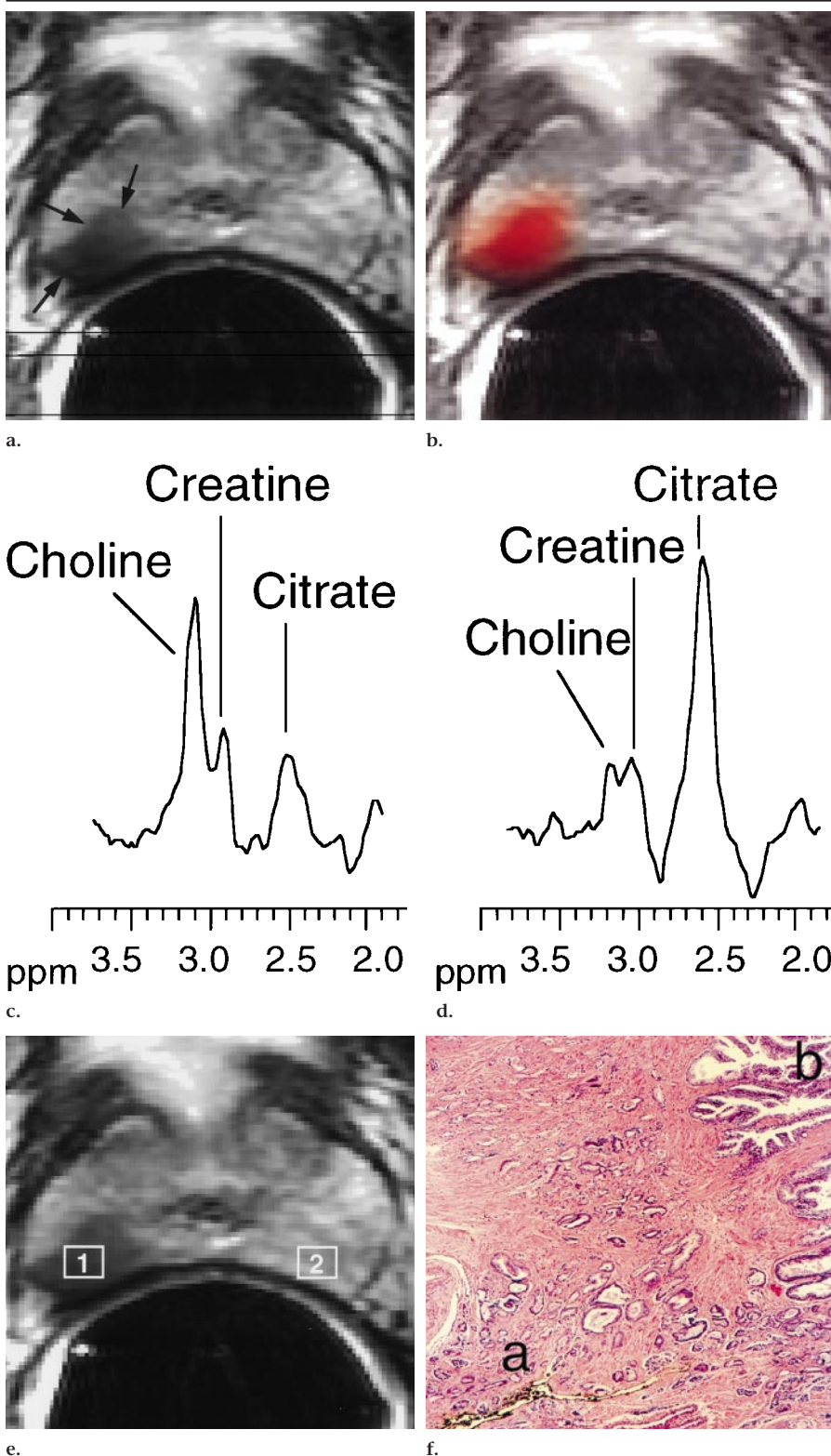


**Figure 2.** Histopathologic stage pT3a prostate cancer, Gleason score 5, in a 58-year-old man. (a) Fast spin-echo T2-weighted (5,000/102) transverse MR image through the middle gland was obtained with an endorectal coil. A tumor focus (arrows) is seen as an area of decreased signal intensity in the peripheral zone of the right gland, and it was detected by both readers. (b) The same section as in a shows areas of definite cancer, as demonstrated with 3D MR spectroscopic imaging findings overlaid in red. Note the concordance between a and b. (c) MR spectrum obtained from area of imaging abnormality (1 in e) in the right peripheral zone demonstrates elevated choline and reduced citrate, a pattern consistent with definite cancer. (d) MR spectrum obtained from a normal left peripheral zone (2 in e) demonstrates a normal spectral pattern with citrate dominant and no abnormal elevation in choline. (e) Fast spin-echo (5,000/102) transverse MR image depicts an area of imaging abnormality in the right peripheral zone (1) and a normal left peripheral zone (2). (f) Photomicrograph of histopathologic section shows tumor in the peripheral zone of the right middle gland, which abuts the inked prostatic margin (a) and is interspersed between normal prostatic glands (b). (Hematoxylin-eosin stain; original magnification,  $\times 100$ .)

patients had low-grade tumors (Gleason score, 2+2) that encompassed less than 5% of the lobe. In the other two cases, the false-negative diagnoses (Gleason scores, 3+3 and 3+4) were due to improper placement of the spectroscopic box, which was placed centrally and did not cover the posterolateral aspect of the peripheral zone.

A false-positive diagnosis of tumor was made with 3D MR spectroscopic imaging in five prostatic lobes. In three cases, the false-positive diagnosis was obtained in early studies with larger voxels, which led to contamination of the spectra from periurethral and central gland tissue. In one case, a single 0.24-cm<sup>3</sup> voxel was positive in a lobe in which no cancer was found at histopathologic examination. In the remaining case, no apparent explanation for the false-positive result could be found.

#### Complementary Role of MR Imaging and 3D MR Spectroscopic Imaging

For ROC analysis of combined MR imaging and 3D MR spectroscopic imaging, results with MR imaging were added to the results with 3D MR spectroscopic imaging, which provided approximately equally weighting for both MR imaging and 3D MR spectroscopic imaging. ROC curves with combined MR imaging and 3D MR spectroscopic imaging are shown in Figure 1. ROC analysis demonstrated

sponding 3D MR spectroscopic imaging results and histopathologic sections. Lowering of the threshold for cancer detection with 3D MR spectroscopic imaging (possible cancer) resulted in ef-

ficacy data similar to those with MR imaging.

False-negative 3D MR spectroscopic imaging results were obtained in four of 106 prostatic lobes. In two of these cases, the

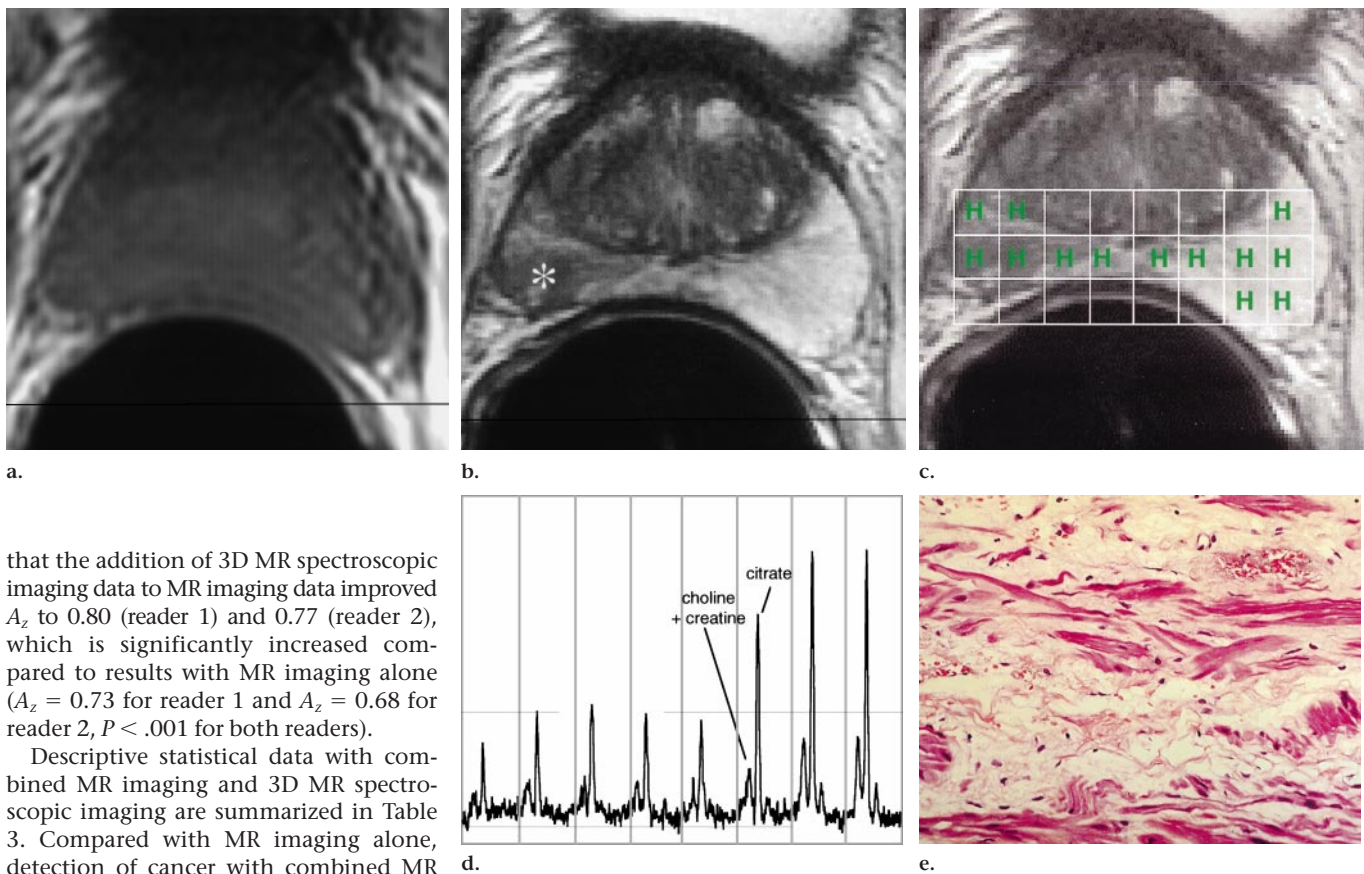


**Figure 3.** Histopathologic stage pT2a prostate cancer, Gleason score 6, in a 54-year-old man. (a) T1-weighted (600/12) transverse MR image through the base of the prostate was obtained with an endorectal coil. No areas of high signal intensity are visible to suggest postbiopsy hemorrhage. (b) Corresponding fast spin-echo T2-weighted (5,000/102) transverse MR image through the middle gland. An area of low signal intensity (\*) in the right middle gland was rated as definite cancer by both readers because it did not represent hemorrhage on the basis of findings in a. (c) The same section, with the information from 3D MR spectroscopic imaging overlaid (H indicates voxels with normal [healthy] metabolic spectra). (d) Selected MR spectra obtained from the middle row of the two-dimensional array in c demonstrate reduced signal intensity in the area of the imaging abnormality. However, the metabolic ratios remain normal. (e) Photomicrograph of the histopathologic section from the area of MR imaging abnormality in the right peripheral zone shows edema, separation of muscle bundles, and extravasated red blood cells, most likely due to transrectal biopsy. No tumor was present in this sextant, which confirms that 3D MR spectroscopic imaging findings had correctly excluded cancer and that the MR imaging findings were misleading. (Hematoxylin-eosin stain; original magnification,  $\times 200$ .)

that the addition of 3D MR spectroscopic imaging data to MR imaging data improved  $A_z$  to 0.80 (reader 1) and 0.77 (reader 2), which is significantly increased compared to results with MR imaging alone ( $A_z = 0.73$  for reader 1 and  $A_z = 0.68$  for reader 2,  $P < .001$  for both readers).

Descriptive statistical data with combined MR imaging and 3D MR spectroscopic imaging are summarized in Table 3. Compared with MR imaging alone, detection of cancer with combined MR imaging and 3D MR spectroscopic imaging (possible or definite cancer) resulted in significantly higher specificity but lower sensitivity, whereas detection of cancer with either MR imaging or 3D MR spectroscopic imaging alone resulted in significantly higher sensitivity but lower specificity. The combination of MR imaging and 3D MR spectroscopic imaging findings that was most predictive of cancer in a sextant (positive predictive value, 89%–92%) was the detection of cancer with both MR imaging and 3D MR spectroscopic imaging ( $>3$  SDs, definite cancer). The combination that was most useful for excluding the presence of cancer in a sextant (negative predictive value, 74%–82%) was the absence of cancer with either MR imaging or 3D MR spectroscopic imaging ( $>2$  SDs, definite or possible cancer).

When cancer was not found with MR imaging, the probability that additional tumor sites would be found with 3D MR spectroscopic imaging was highest when the less stringent 3D MR spectroscopic imaging criteria for defining cancer were used ( $>2$  SDs, possible or definite cancer). For both readers, the probability that additional tumor sites would be found with 3D MR spectroscopic imaging was approximately 50%–80% (95% CI). The

addition of 3D MR spectroscopic imaging to MR imaging also contributed to the exclusion of tumor. The probability of identification of additional sites of normal prostatic tissue when 3D MR spectroscopic imaging results ( $>3$  SDs, definite cancer) were added to MR imaging results was 47%–79% and 62%–87% (95% CI) for readers 1 and 2, respectively.

## DISCUSSION

MR imaging continues to evolve in the diagnostic evaluation of prostate cancer. It has found a role as a local staging

modality for differentiation between patients with organ-confined cancer and those with extracapsular tumor extension (20–27). New treatment strategies (eg, imaging-guided brachytherapy [28–30], laser therapy [31], and cryotherapy [32,33]) and the concept of watchful waiting (34) require an extension of diagnostic imaging beyond staging to providing more precise information about tumor presence and location. Accurate tumor localization will allow greater intensity of treatment to areas of the prostate gland where cancer is present, which will ideally increase the effectiveness of treatment while reducing treatment-related morbidity.

**TABLE 3**  
**Findings with Combined MR Imaging and 3D MR Spectroscopic Imaging for Tumor Detection and Localization on a Sextant-by-Sextant Basis (right and left base, middle gland, apex)**

Modality and Finding	Sensitivity (%)	Specificity (%)	Positive Predictive Value (%)	Negative Predictive Value (%)	Accuracy (%)
<b>MR imaging, positive and 3D MRSI, definite</b>					
Reader 1	52 (80 of 155)*	91 (72 of 79)†	92 (80 of 87)	49 (72 of 147)	65 (152 of 234)
95% CI	45, 58	87, 95	88, 95	43, 55	59, 71
Reader 2	55 (85 of 155)*	87 (69 of 79)†	89 (85 of 95)	50 (69 of 139)	66 (154 of 234)
95% CI	48, 61	83, 92	86, 93	43, 56	60, 72
<b>MR imaging, positive or 3D MRSI, definite</b>					
Reader 1	89 (138 of 155)†	44 (35 of 79)*	76 (138 of 182)	67 (35 of 52)	74 (173 of 234)
95% CI	85, 93	38, 51	70, 81	61, 73	68, 80
Reader 2	89 (138 of 155)†	33 (26 of 79)*	72 (138 of 191)	60 (26 of 43)	70 (164 of 234)
95% CI	85, 93	27, 39	67, 78	54, 67	64, 76
<b>MR imaging, positive and 3D MRSI, possible</b>					
Reader 1	68 (106 of 155)	80 (63 of 79)†	87 (106 of 122)	56 (63 of 112)	72 (169 of 234)
95% CI	62, 74	75, 85	83, 91	50, 63	66, 78
Reader 2	73 (113 of 155)	70 (55 of 79)†	82 (113 of 137)	57 (55 of 97)	72 (168 of 234)
95% CI	67, 79	64, 76	78, 87	50, 63	66, 78
<b>MR imaging, positive or 3D MRSI, possible</b>					
Reader 1	95 (148 of 155)†	41 (32 of 79)*	76 (148 of 195)	82 (32 of 39)	77 (180 of 234)
95% CI	93, 98	34, 47	70, 81	77, 87	72, 82
Reader 2	94 (146 of 155)†	33 (26 of 79)*	73 (146 of 199)	74 (26 of 35)	74 (172 of 234)
95% CI	91, 97	27, 39	68, 79	69, 80	68, 79

Note.—MRSI = MR spectroscopic imaging. Data in parentheses are the number of prostatic lobes.

\*  $P < .05$ , lower than MR imaging.

†  $P < .05$ , higher than MR imaging.

In addition, information about tumor growth with accurate tumor localization and sizing may also assist selection and maintenance of a watchful waiting strategy that may obviate repeated biopsies. Knowledge of tumor location may also be of use in patients with elevated prostate-specific antigen level but repeatedly negative findings at prostatic biopsy. In that clinical setting, knowledge of tumor location may help guide future biopsies.

Current diagnostic strategies have limitations in tumor detection and localization. Transrectal US fails to depict as many as 8%–30% of lesions palpable at digital rectal examination. Transrectal US also has a high false-positive rate in cancer evaluation because only 20% of hypoechoic lesions (US finding most indicative of cancer) are malignant (35,36). MR imaging with a combined endorectal and phased-array coil has demonstrated a high sensitivity (91%) but low specificity (27%) in tumor lateralization (5). Initial reports about 3D MR spectroscopic imaging show that the ability of this technique to distinguish between cancer, benign prostatic hypertrophy, and normal prostatic tissue suggests that the addition of 3D MR spectroscopic imaging to clinical MR imaging may increase the specificity of MR imaging in tumor detection and localization

(13,37). In this study, we evaluated this hypothesis by correlating results with MR imaging, 3D MR spectroscopic imaging, or both to those with step-section histopathologic examination in patients who underwent prostatectomy.

Data points on the ROC curve indicated a significantly better performance with combined MR imaging and 3D MR spectroscopic imaging than with MR imaging alone. With use of various combinations of MR imaging and 3D MR spectroscopic imaging, a point on the ROC curve can be chosen that provides either high sensitivity or high specificity depending on clinical requirements. Three-dimensional MR spectroscopic imaging demonstrated a significantly higher specificity in tumor localization than did MR imaging. A positive result with combined MR imaging and 3D MR spectroscopic imaging (>3 SDs) indicated the presence of tumor with high probability (positive predictive value, 89%–92%), whereas a negative result (>2 SDs) excluded the presence of cancer with high probability (negative predictive value, 74%–82%).

Findings in the preliminary study by Vigneron et al (38) suggest that small, low-grade tumors may be undetected with 3D MR spectroscopic imaging because the severity of metabolite alteration corre-

lates with tumor aggressiveness. High-grade cancers (Gleason scores 7 and 8) revealed highly elevated choline resonances, whereas lower grade tumors (Gleason scores 4 and 5) showed slightly elevated choline levels only (38). Other reasons for wrong 3D MR spectroscopic imaging results in our pilot study, such as box placement errors and spectral contamination in large voxels, can now be avoided. The experience gained with 3D MR spectroscopic imaging has led to standardization of the technique and important progress in the development of 3D MR spectroscopic imaging as a clinically useful tool. During the period of this study, technical developments resulted in improved spatial resolution (from 0.7 to 0.24 cm<sup>3</sup>), complete gland coverage, and reduction in total examination time (for both MR imaging and 3D MR spectroscopic imaging).

In conclusion, findings in this study demonstrate the potential usefulness of combined morphologic and metabolic information about prostate cancer in clinical practice and provide an analysis of this new method. Our findings show that the addition of 3D MR spectroscopic imaging to MR imaging provides better detection and localization of prostate cancer in a sextant of the prostate, with

sensitivity and specificity higher than those with MR imaging alone.

## References

1. Silverberg E. Cancer statistics, 1985. *CA Cancer J Clin* 1985; 35:19-35.
2. Wingo PA, Landio S, Ries LAG. An adjustment to the 1997 estimate for new prostate cancer cases. *CA Cancer J Clin* 1997; 47:239-242.
3. Waterbor JW, Bueschen AJ. Prostate cancer screening (United States). *Cancer Causes Control* 1995; 6:267-274.
4. Parker SL, Tong T, Bolden S, Wingo PA. Cancer statistics, 1997. *CA Cancer J Clin* 1997; 47:5-27.
5. Hricak H, White S, Vigneron D, et al. Carcinoma of the prostate gland: MR imaging with pelvic phased-array coils versus integrated endorectal—pelvic phased-array coils. *Radiology* 1994; 193:703-709.
6. Jager GJ, Ruijter ET, van de Kaa CA, et al. Local staging of prostate cancer with endorectal MR imaging: correlation with histopathology. *AJR* 1996; 166:845-852.
7. Presti JC Jr, Hricak H, Narayan PA, Shinohara K, White S, Carroll PR. Local staging of prostatic carcinoma: comparison of transrectal sonography and endorectal MR imaging. *AJR* 1996; 166:103-108.
8. Quint LE, Van Erp JS, Bland PH, et al. Carcinoma of the prostate: MR images obtained with body coils do not accurately reflect tumor volume. *AJR* 1991; 156:511-516.
9. Sommer FG, Nghiem HV, Herfkens R, McNeal J, Low RN. Determining the volume of prostatic carcinoma: value of MR imaging with an external-array coil. *AJR* 1993; 161:81-86.
10. White S, Hricak H, Forstner R, et al. Prostate cancer: effect of postbiopsy hemorrhage on interpretation of MR images. *Radiology* 1995; 195:385-390.
11. Evanochoko WT, Ng TC, Glickson JD. Application of in vivo NMR spectroscopy to cancer. *Magn Reson Med* 1984; 1:508-534.
12. Bruhn H, Frahm J, Gyngell ML, et al. Noninvasive differentiation of tumors with use of localized H-1 MR spectroscopy in vivo: initial experiments in patients with cerebral tumors. *Radiology* 1989; 172:541-548.
13. Kurhanewicz J, Vigneron DB, Hricak H, Narayan P, Carroll P, Nelson SJ. Three-dimensional H-1 MR spectroscopic imaging of the in situ human prostate with high (0.24-0.7-cm<sup>3</sup>) spatial resolution. *Radiology* 1996; 198:795-805.
14. Chen M, Hricak H, Kalbhen CL, et al. Hormonal ablation of prostatic cancer: effects on prostate morphology, tumor detection, and staging by endorectal coil MR imaging. *AJR* 1996; 166:1157-1163.
15. Vigneron DB, Nelson SJ, Moyher S, Kelley DAC, Kurhanewicz J, Hricak H. An analytical correction of MR images obtained with endorectal or surface coils (abstr). *JMRI* 1993; 3(P):142.
16. Kurhanewicz J, Vigneron DB, Hricak H, et al. Prostate cancer: metabolic response to cryosurgery as detected with 3D H-1 MR spectroscopic imaging. *Radiology* 1996; 200:489-496.
17. Star-Lack J, Nelson SJ, Kurhanewicz J, Huang LR, Vigneron DB. Improved water and lipid suppression for 3D PRESS CSI using RF band selective inversion with gradient dephasing (BASING). *Magn Reson Med* 1997; 38:311-321.
18. Dwyer AJ. Matchmaking and McNemar in the comparison of diagnostic modalities. *Radiology* 1991; 178:328-330.
19. Hanley JA, McNeil BJ. A method of comparing the areas under receiver operating characteristic curves derived from the same cases. *Radiology* 1983; 148:839-843.
20. Yu KK, Hricak H, Alagappan R, Chernoff DM, Bacchetti P, Zaloudek CJ. Detection of extracapsular extension of prostate carcinoma with endorectal and phased-array coil MR imaging: multivariate feature analysis. *Radiology* 1997; 202:697-702.
21. Schiebler ML, Yankaskas BC, Tempany C, et al. MR imaging in adenocarcinoma of the prostate: interobserver variation and efficacy for determining stage C disease. *AJR* 1992; 158:559-564.
22. Tempany CM, Zhou X, Zerhouni EA, et al. Staging of prostate cancer: results of Radiology Diagnostic Oncology Group project comparison of three MR imaging techniques. *Radiology* 1994; 192:47-54.
23. Seltzer SE, Getty DJ, Tempany CM, et al. Staging prostate cancer with MR imaging: a combined radiologist-computer system. *Radiology* 1997; 202:219-226.
24. Outwater EK, Petersen RO, Siegelman ES, Gomella LG, Chernesky CE, Mitchell DG. Prostate carcinoma: assessment of diagnostic criteria for capsular penetration on endorectal coil MR images. *Radiology* 1994; 193:333-339.
25. Harris RD, Schned AR, Heaney JA. Staging of prostate cancer with endorectal MR imaging: lessons from a learning curve. *RadioGraphics* 1995; 15:813-832.
26. Schnell MD, Imai Y, Tomaszewski J, Pollack HM, Lenkinski RE, Kressel HY. Prostate cancer: local staging with endorectal surface coil MR imaging. *Radiology* 1991; 178:797-802.
27. Tempany CM, Rahmouni AD, Epstein JI, Walsh PC, Zerhouni EA. Invasion of the neurovascular bundle by prostate cancer: evaluation with MR imaging. *Radiology* 1991; 181:107-112.
28. Ragde H, Blasko JC, Grimm PD, et al. Interstitial iodine-125 radiation without adjuvant therapy in the treatment of clinically localized prostate carcinoma. *Cancer* 1997; 80:442-453.
29. Stokes SH, Real JD, Adams PW, Clements JC, Wuertzer S, Kan W. Transperineal ultrasound-guided radioactive seed implantation for organ-confined carcinoma of the prostate. *Int J Radiat Oncol Biol Phys* 1997; 37:337-341.
30. Stone NN, Stock RG. Brachytherapy for prostate cancer: real-time three-dimensional interactive seed implantation. *Tech Urol* 1995; 1:72-80.
31. Amin Z, Lees WR, Bown SG. Technical note: interstitial laser photocoagulation for the treatment of prostatic cancer. *Br J Radiol* 1993; 66:1044-1047.
32. Lee F, Bahn DK, McHugh TA, Onik GM, Lee FT Jr. US-guided percutaneous cryoablation of prostate cancer. *Radiology* 1994; 192:769-776.
33. Onik GM, Cohen JK, Reyes GD, Rubinsky B, Chang Z, Baust J. Transrectal ultrasound-guided percutaneous radical cryosurgical ablation of the prostate. *Cancer* 1993; 72:1291-1299.
34. Chodak GW, Thisted RA, Gerber GS, et al. Results of conservative management of clinically localized prostate cancer. *N Engl J Med* 1994; 330:242-248.
35. Lee F, Torp-Pedersen S, Littrup PJ, et al. Hypoechoic lesions of the prostate: clinical relevance of tumor size, digital rectal examination, and prostate-specific antigen. *Radiology* 1989; 170:29-32.
36. Olsson C. Prostatic cancer. *Kidney Int* 1993; 43:955-965.
37. Kurhanewicz J, Vigneron DB, Nelson SJ, et al. Citrate as an in vivo marker to discriminate prostate cancer from benign prostatic hyperplasia and normal prostate peripheral zone: detection via localized proton spectroscopy. *Urology* 1995; 45:459-466.
38. Vigneron DB, Males R, Noworolski S, et al. 3D MRSI of prostate cancer: correlation with histologic grade (abstr). In: Proceedings of the Sixth Meeting of the International Society for Magnetic Resonance in Medicine. Berkeley, Calif: International Society for Magnetic Resonance in Medicine, 1998; 487.